International Journal of Applied Science and Engineering

The effect of model scale, acceleration history, and soil condition on closed-ended pipe pile response under coupled static-dynamic loads

Duaa Al-Jeznawi[1], I. B. Mohamed Jais[2*], Bushra S. Albusoda[3]

[1] *PhD Candidate, School of Civil Engineering, College of Engineering, Universiti Teknologi MARA Shah Alam; Lecturer at College of Engineering, Al-Nahrain University, Baghdad, Iraq.*
[2] *Senior Lecturer, School of Civil Engineering, College of Engineering, Universiti Teknologi MARA Shah Alam, 40450, Selangor, Malaysia.*
[3] *University of Baghdad, College of Engineering, Iraq*

ABSTRACT

This paper analyzes the effect of scaling-up model and acceleration history on seismic response of closed-ended pipe pile using a finite element modeling approach and the findings of 1 g shaking table tests of a pile embedded in dry and saturated soils. A number of scaling laws were used to create the numerical modeling according to the data obtained from 1 g shake table tests performed in the laboratory. The current study found that the behaviors of the scaled models, in general have similar trends. From numerical modeling on both the dry and saturated sands, the normalized lateral displacement, bending moment, and vertical displacement of piles with scale factors of 2 and 35 are less than those of the pile with a scale factor of 1 and the shaking table test. In general, the pile deformation factor was higher in saturated sand models than the dry sand models. Liquefaction ratios were increased by increasing the seismic intensity; hence the maximum liquefaction ratio was observed with the model of scale 1 under the effect of the Kobe earthquake (0.82 g). In another full-scale model, the liquefaction ratio decreased significantly; i.e., it was decreased from 1.64% (λ=1) to 1.04% (λ=35) in the same mentioned model. Pile frictional resistance was numerically investigated and the overall results were compared with previous studies in the literature. In general, the frictional resistance at the pile tip was slightly higher than the frictional resistance around the pile body, and the frictional resistance factor on the ground surface of dry soil models was slightly higher than those of saturated soil models.

Keywords: Model scale, Acceleration history, Soil-pile interaction, Modeling, Seismic excitation.

OPEN ACCESS

Received: February 7, 2022
Revised: March 25, 2022
Accepted: March 30, 2022

Corresponding Author:
I. B. Mohamed Jais
ismac821@uitm.edu.my

Publisher:
Chaoyang University of Technology
ISSN: 1727-2394 (Print)
ISSN: 1727-7841 (Online)

1. INTRODUCTION

Although pile foundations in many cases experienced liquefaction-induced deformations of significant magnitude, in 1995 Kobe earthquake revealed that the large ground displacements may cause huge damage to piles, as shown in Fig. 1 (Takashi and Gazetas, 1996). Since then, it has been taken years and a lot of money to detect the damage, as piles are embedded in the ground. A few works investigated the performance of pile foundations under seismic excitation, and while their findings were useful, they were still not enough to uncover the geotechnical performance features. The intensity of deformation somewhere at the contact of various soil strata is connected to their nonlinear, pressure experienced behavior during ground shaking, and is the most important component influencing the seismic soil-pile coupling (Hussein and El-Naggar (2021), Almashhadany and Albusoda (2014)). A Shaking table test is generally used to study the soil-pile system since it can simulate various soils, different types of piles,

and can induce real seismic excitation. Tokimatsu et al. (2004) conducted large-scale shaking table tests in dry and saturated soils to examine the kinematic and inertial forces on piles under earthquakes. The findings revealed that the superstructure's natural period was longer than the soil. Once the natural period of the superstructure is longer than the soil, inertial and kinematic factors affect pile stresses. Yasuda et al. (2000) used full-scale piles embedded in horizontal and sloping ground to conduct large-scale shaking table tests. They showed that the interface between the pile and the foundation in horizontal surface and the liquefaction-induced ground movement in sloped ground governed the piles' behavior. Ebeido et al. (2019) used a 3% inclined layer of sand with a relative density of 40%–50% to perform four large scales shaking table tests to investigate the behavior of single pipe piles made of steel and pile groups to liquefaction-induced differential settlement. The largest bending moment was observed at the commencement of the liquefaction, and the irreversible pile deformation was less than the maximum deformation may be attributed to partial pile rebound.

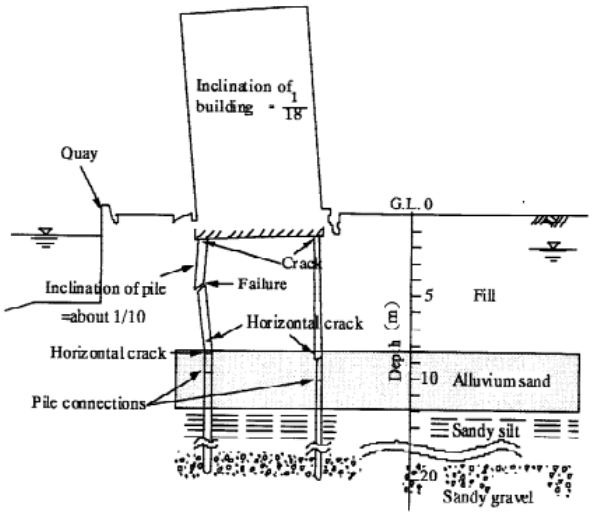

Fig. 1. After the Kobe earthquake (1995), damage of pile foundation by liquefaction (Oh-oka et al. 1996)

The Iraqi area has been more seismically active in recent decades, prompting local academics to study pile foundations in sandy soil during various kinds of earthquake motions (Al-Tameemi, 2018; Al-Ghanim, 2019; Al-Ghanim et al., 2019; Al-Salakh and Albusoda, 2020; Al-Jeznawi et al., 2022a). Al-Tameemi (2018) used flexible laminar shaking table experiments and FLAC 3D computer modeling with various pile dimensions and actual earthquake vibrations, from weak to extremely severe, at varying factors of safety to investigate the impacts on single piles during different earthquake histories. He observed that pile settlement in loose sand went up dramatically as the earthquake's acceleration increased, but pile lateral displacement peaked at maximum acceleration and remained unchanged throughout the earthquake. Additionally, the numerical model utilizing FLAC 3D was also found to be suitable for estimating liquefaction depending on pore pressure development and dissipation during dynamic excitation.

Pipe piles are widely used due to: costs can be reduced since they can be adapted to exact load standards; pipe piles save money by eliminating the need for additional structural support; they are cheaper and simpler to create; and they may be evaluated and safety tested prior to getting installed. Hussein and Albusoda (2021a, and 2021b) performed several shaking table tests to investigate the following: the effect of combined axial and lateral loadings in liquefiable and non-liquefiable soil and the effect of different excitation intensities on soil-pile interaction. Thus, the current study is focused on numerical modeling of the effect of scaling factors (scale 1, 2, and 35 (full scale)), acceleration histories (Kobe, Ali Algharbi, and Halabja earthquake), and soil conditions (dry and saturated) on closed-ended pipe pile response under coupled static- dynamic loads.

2. SCALING LAW

Although full-scale models provide the most accurate portrayal of foundation behavior in various subsoil conditions, particularly sand, they are expensive and time-consuming to develop. To control the research program's cost and time limitations, geotechnical small-scale prototypes are used (Hussein and El-Naggar, 2021). Since these scaled models were able to capture the essential results from the experiment with precision, the findings had to be extrapolated to the original scale. Because there are numerous elements govern the soil-foundation models, that affects the generalization process of the findings, correlation criteria should be implemented to develop an accurate model. Nonlinear soil behavior, multiple-layer interface, and non - homogeneous soil characteristics are all noteworthy factors. The main aim of the shaking table model scale is to establish dynamic comparability, which means that both the full-scale model and the tested model have homogeneous forces. Wood (2004) presented a package of scaling variables for the soil-pile model in a 1 g shaking table test, including scaling for length, time, stress, density, displacement, bending moment, forces, and much more. The key model similitude characteristics are expressed in terms of the geometric scaling factor λ. The intended model was scaled up using a geometry factor 'λ' to study the soil-pile behavior and compare the results with the actual scale of the laboratory test, which was performed by Hussein and Albusoda (2021a and 2021b). The pile scaling and soil layers obeyed the scaling laws, where the later are described and summarized in Table 1. The density factor is equal to unity because the soil strata in the lab sample and the numerical model are intended to be equivalent, and the acceleration factor is also 1.0 because the 1 g shaking table test is conducted in a natural gravity. As a result, the scaled models can gather the appropriate data in this study from 1

g shaking table test, which then be extended to the different-scale models.

Subsequently, the earthquake duration was scaled-up by multiplying the original acceleration time to $\lambda^{0.75}$, and then the intended acceleration values were incorporated with the scaled time set. Table 2 summarizes the input scaled parameters for the current numerical models.

Table 1. Scaling parameters (Wood, 2004)

Quantity	General	Scale factor 1 g prototype/model
Length	λ_L	$1/\lambda$
Density	λ_ρ	1
Acceleration	λ_g	1
Time (Dynamic)	λ_T	$1/\lambda^{(1-\frac{\alpha}{2})}$
Force	$\lambda_g \lambda_\rho \lambda^3_L$	$1/\lambda^3$
Stiffness	λ_G	$1/\lambda^\alpha$
Stress	$\lambda_\rho \lambda_g \lambda_L$	$1/\lambda$
Strain	$\lambda_\rho \lambda_g \lambda_L/ \lambda_G$	$1/\lambda^{1-\alpha}$
Displacement	$\lambda_\rho \lambda_g \lambda_L^2/ \lambda_G$	$1/ \lambda$
Permeability (Darcy's law)	$\lambda_{\rho f} \lambda_g/ \lambda_v$	1
Velocity	$\lambda_g \lambda_L(\lambda_\rho/ \lambda_G)^{0.5}$	$1/\lambda^{(1-\frac{\alpha}{2})}$
Bending moment/unit length	$\lambda_g \lambda_\rho \lambda^3_L$	$1/ \lambda^3$

Table 2. The main scaled input parameters

Input parameter	Scale 1 (λ =1)	Scale 2 (λ =2)	Scale 35 (Full scale model)
Time (sec.)	48 (Kobe) 159 (Ali Algharbi) 300 (Halabja)	80 267 504	690 2288 4317
Pile's cross section area (m)	6.8E-5	2.7E-4	8.4E-2
Pile length (m)	0.5	1.0	17.5
Soil box dimensions (m)	0.6 × 0.6 × 0.8	1.2 × 1.2 × 1.8	21 × 21 × 28
Cap pile dimensions (m)	0.05 × 0.05 × 0.01	0.1 × 0.1 × 0.02	1.75 × 1.75 × 0.35
Vertical load (N)-50% of allowable pile capacity	32.5 (dry) 19.6 (saturated)	260 (dry) 156.8 (saturated)	1.4E6 (dry) 0.84E6 (saturated)
Lateral load (N)- 50% of allowable pile capacity	3.5(dry) 1.96 (saturated)	28 (dry) 15.7 (saturated)	1.5E5 (dry) 0.84E5 (saturated)

3. SOIL-PILE MODEL DESCRIPTION

Fig. 2 illustrates the configuration of soil-pile full scale model which was implemented in this study. As for the saturated models, the water table was maintained at the ground level. The 3-D soil-pile model was developed using MIDAS GTS NX software to model the nonlinear behavior under the effect of static-dynamic loads. The current constitutive model is calibrated and compared with the findings of the shaking table test program by Hussein and Albusoda (2021a and 2021b). The dimension of soil box exceeded the minimal lateral bounds on the piles' lateral behavior according to the elastic concept (i.e., 17d) and matched the impact area limitation (Robinsky and Morrison, 1964). Even though vertical boundaries do not influence on piles' seismic lateral behavior (Dong et al., 2018), the current model was designed such that maintained the distance to the bottom boundary exceeding 4*pile diameter. To improve the soil-pile interaction in the lateral and vertical directions, the soil elements close to the pile body were properly adjusted and refined. The mesh elements were also segmented to allow the shear wave to go effectively through the soil layers. The material geotechnical properties were correlated using the physical data of the soil utilized in the shaking table test, and the correlation was carried out during the calibration process to match the exact soil-pile behavior.

For full scale model, the pile was 0.56 m in diameter (outside diameter), 0.105 m thick, and 17.5 m long, and its tip was situated at 11.5 m above the soil bottom. The soil box had dimensions (X, Y, Z) of 21 m × 21 m x 28 m, respectively. The pile was connected to the aluminum cap with dimensions of 1.75 m × 1.75 m × 0.35 m. A very fine mesh was used to capture the attitude of soil-pile interaction under different seismic excitations with 4 nodes tetrahedral elements.

Three construction stages were established via MIDAS GTS NX for nonlinear static and nonlinear time history analyses; the first stage was for calculating the model self-weight, the second stage was for calculating combined static loads, and a third stage for applying the dynamic load (earthquake). Static boundary conditions were considered for the first and second stages, as for the dynamic analysis,

new elements were adapted to create the ground surface spring (provided elastic boundary conditions) and free field elements were created in the direction of applying the earthquake.

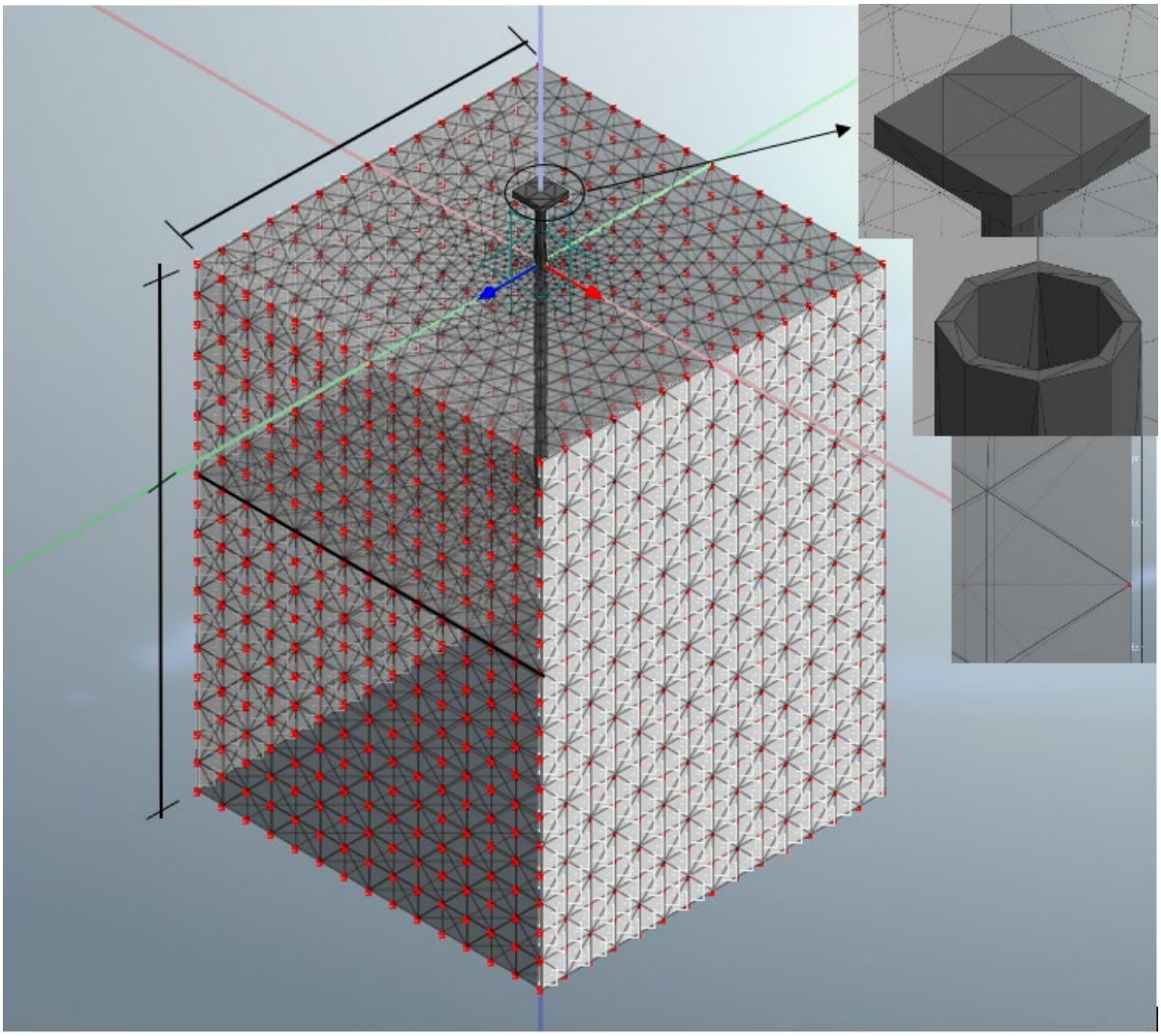

Fig. 2. Configuration of soil-pile full scale model

4. MATERIALS DESCRIPTION

The potential of the soil constitutive model to anticipate the exact attitude of the soil during dynamic loading is a fundamental component defining the quality of any numerical model used in soil dynamics. Since this research aims to investigate the interaction effect of the soil-pile system under a coupled of static-dynamic load to demonstrate the influence of the main parameters, a modified Mohr-Coulomb model was adopted for the dry soil layers and modified UBCSAND model (Beaty and Byrne, 2011) was used to simulated the saturated soil layers. Input parameters were adjusted based on the scaling factors (1, 2, 35 (full scale)), and these parameters were initially extrapolated from 1 g shaking table tests, performed by Hussein and Albusoda (2021a, 2021b). Thus, details of the main parameters implemented in this study are obtained from Hussein and Albusoda (2021a, 2021b) and then calibrated based on Beaty and Byrne (2011). Table 3 and 4 summarized the main calibrated parameters which used in the current numerical modeling. The main calibration equations (Beaty and Byrne, 2022) are based on the equivalent SPT blow count for clean sand $(N_1)_{60,}$ which in turn calculated according to the ASTM D 1586-99.

This modified Mohr-Coulomb concept is an enhancement on the Mohr-Coulomb model, which was created by merging nonlinear elastic and elasto-plastic concepts to create a model that is ideal for silt or sand-based ground's behavioral features. The double stiffening characteristic can be simulated using the Modified Mohr-Coulomb model, which is unaffected by shear failure or compressive yielding. The early deviatory stress causes axial strain and a decrease in mechanical properties, similar to the Hyperbolic (nonlinear elastic) model, but that is close

to the plastic hypothesis than the elastic one, with distinctions in dilatancy angle analysis and yield cap implementation.

As for the modified UBCSAND model, this model is a well-organized stress approach to estimate sand liquefaction during seismic event. Post-peak strain softening with a behavior that is based on the mechanism of a nonlinear failure envelope that is stress dependent, and a modified flow rule that is based on the pattern of shear deformation have all been added to the modified UBCSAND concept. Through using implicit technique, the GTS NX liquefaction concept has been extended to a full 3D implementation of the updated UBCSAND model. The elastic modulus fluctuates depend on the effective stress exerted in the elastic zone, allowing nonlinear elastic behavior to be modeled. Three forms of yield functions describe the behavior in the plastic zone: shear (shear hardening), compression (cap hardening), and pressure cut-off. The influence of soil densification can be properly considered by cyclic loading in the case of shear hardening.

5. RESULTS AND DISCUSSIONS

5.1 Liquefaction Observation

In general, when the excess pore water pressure (u_e) approaches the targeted soil's initial vertical effective stress, the soil loses its shear strength and softens.

Table 3. The main input of dry soil parameters (Hetrogenous soil layers)

Name	Loose sand	Dense sand
Material	Isotropic	Isotropic
Model Type	Modified MC	Modified MC
Poisson's Ratio (ν)	0.33	0.33
Unit Weight (γ) [KN/m^3]	13.5	16
K_o	0.47	0.426
Young Modulus [kPa]	10,525	27,340
Secant Elastic Modulus in Shear Hardening [kPa]	5,639	15,037
Tangential Stiffness Primary Oedometer test loading (E_{oedref}) [kPa]	5,639	15,038
Elastic Modulus at unloading (E_{urref}) [kPa]	16,917	45,111
Failure Ratio (R_f) [%]	0.9	0.9
Porosity [%]	0.6	0.8
Power of Stress Level Dependency (m)	0.5	0.5
Friction Angle [°]	32	35
Dilatancy Angle [°]	2	5
Cohesion (c) [kPa]	0.1	0.1

Table 4. The main input of saturated soil parameters (Hetrogenous soil layers)

Parameter	**Loose sand**	**Dense sand**
Material	Isotropic	Isotropic
Model Type	Modified UBCSAND	Modified UBCSAND
Poisson's Ratio (ν)	0.0163	0.0163
Overburden Pressure [kPa]	102	182
SPT (N-value)	11	17
Equivalent SPT blow count for clean sand $(N_1)_{60}$	9	16
Reference pressure [kPa]	101	101
Elastic shear modulus number [unitless]	902	1093
Elastic shear modulus exponent [unitless]	0.5	0.5
Peak Friction Angle [°]	34	35
Constant Volume Friction Angle [°]	33	33
Cohesion [kPa]	1	1
Plastic shear modulus number [unitless]	320	940
Plastic shear modulus exponent [unitless]	0.4	0.4
Failure ratio	0.79	0.73
Post Liquefaction Calibration Factor (Residual shear modulus) *	0.02	0.7
Soil Densification Calibration Factor (Cyclic Behaviour)	0.45	0.45
Plastic/Pressure cut-off (Tensile Strength kPa)	0	0
Effective unite weight [kN/m^3]	9.11	9.5

**If the max possible stress ratio is achieved, liquefaction is developed and the plastic shear modulus number is decreased by Post Liquefaction Calibration Factor.*

Figs. 4, 5, and 6 show the pore water pressure ratio with time considering different scaling factors (1, 2, 35 (full scale)) and different acceleration histories (Kobe, Ali Algharbi, and Halabja earthquakes). The seismograms of these three earthquakes are shown in Fig. 3.

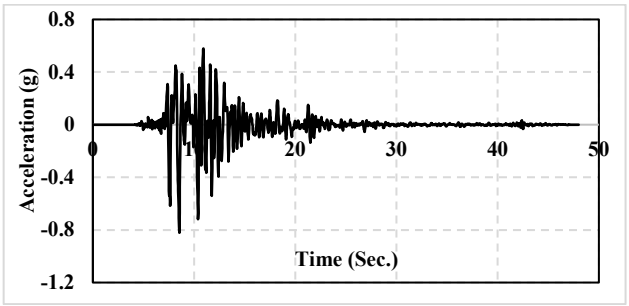

(a) Kobe earthquake

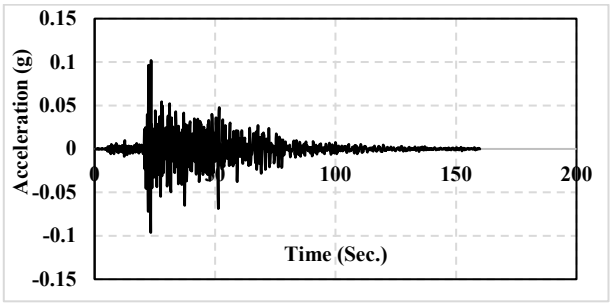

(b) Ali Algharbi earthquake

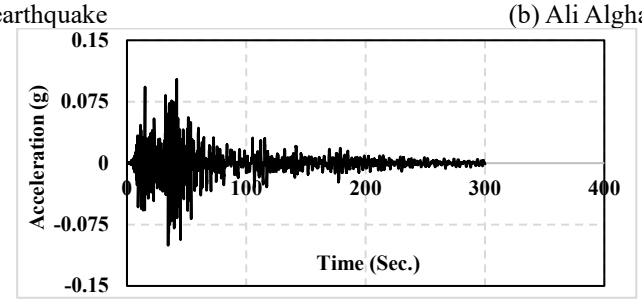

(c) Halabja earthquake

Fig. 3. The seismograms of the used earthquake histories

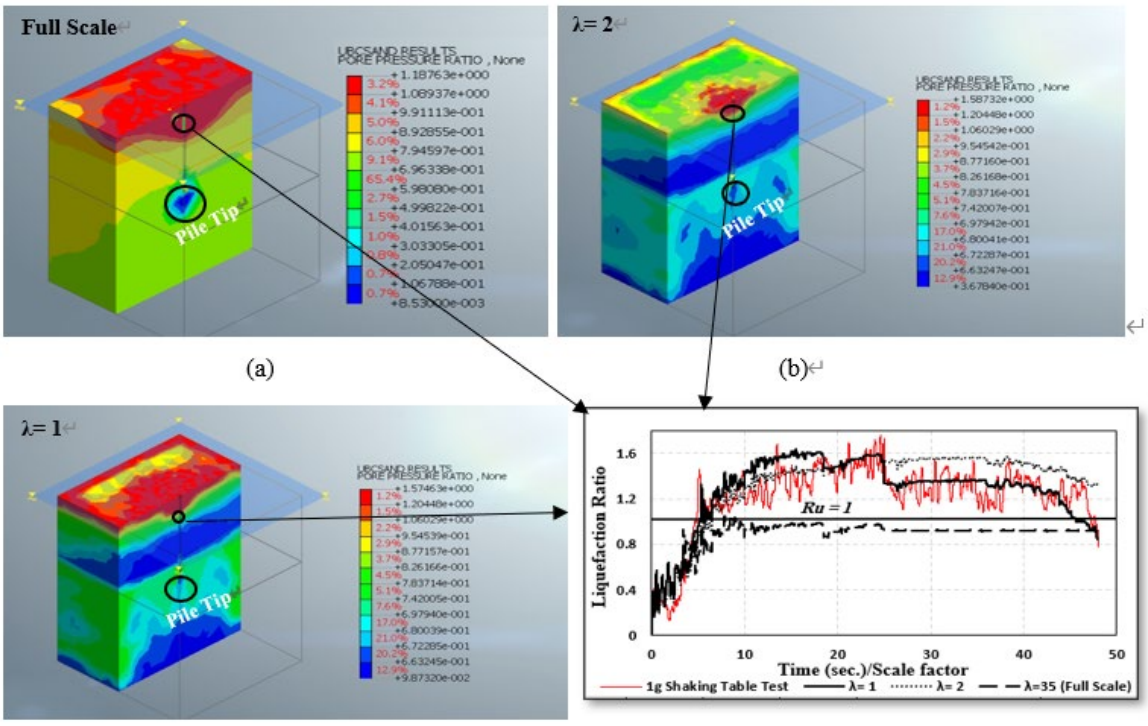

Fig. 4. Liquefaction ratio time history at a specific depth below the ground surface (at the position of maximum excess pore pressure) and under the effect of the Kobe earthquake

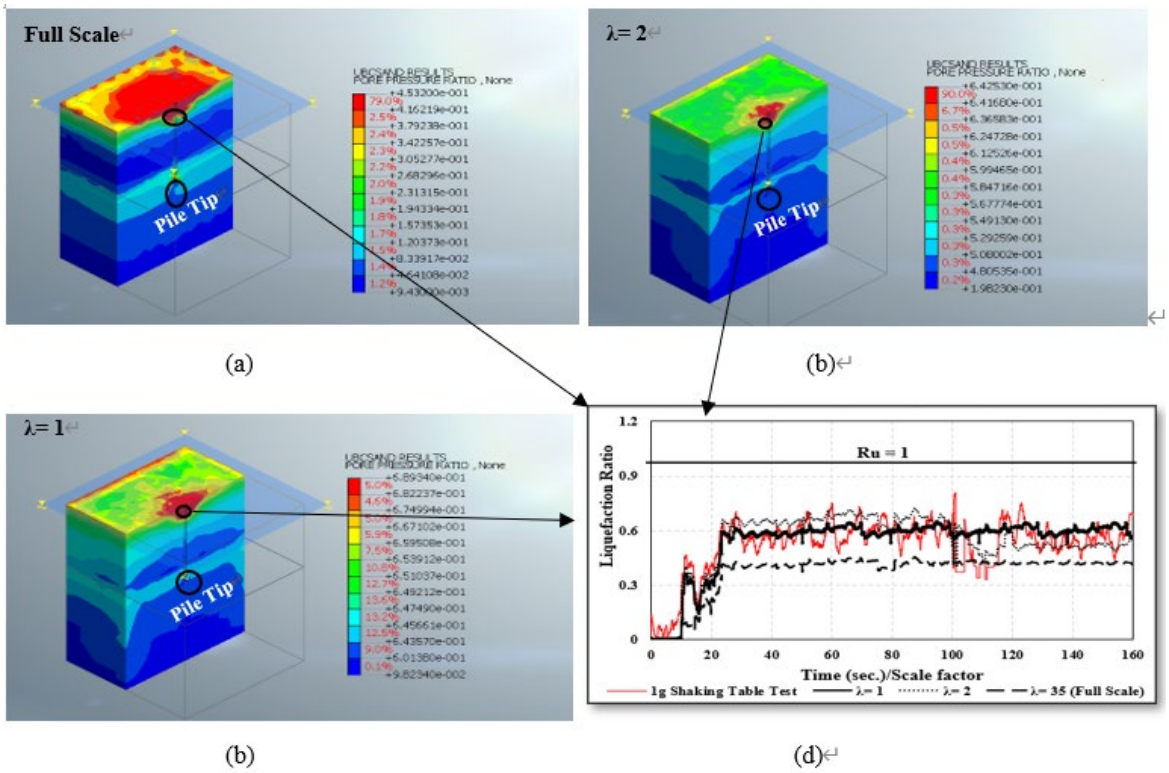

Fig. 5. Liquefaction ratio time history at a specific depth below the ground surface (at the position of maximum excess pore pressure) and under the effect of the Ali Algharbi earthquake

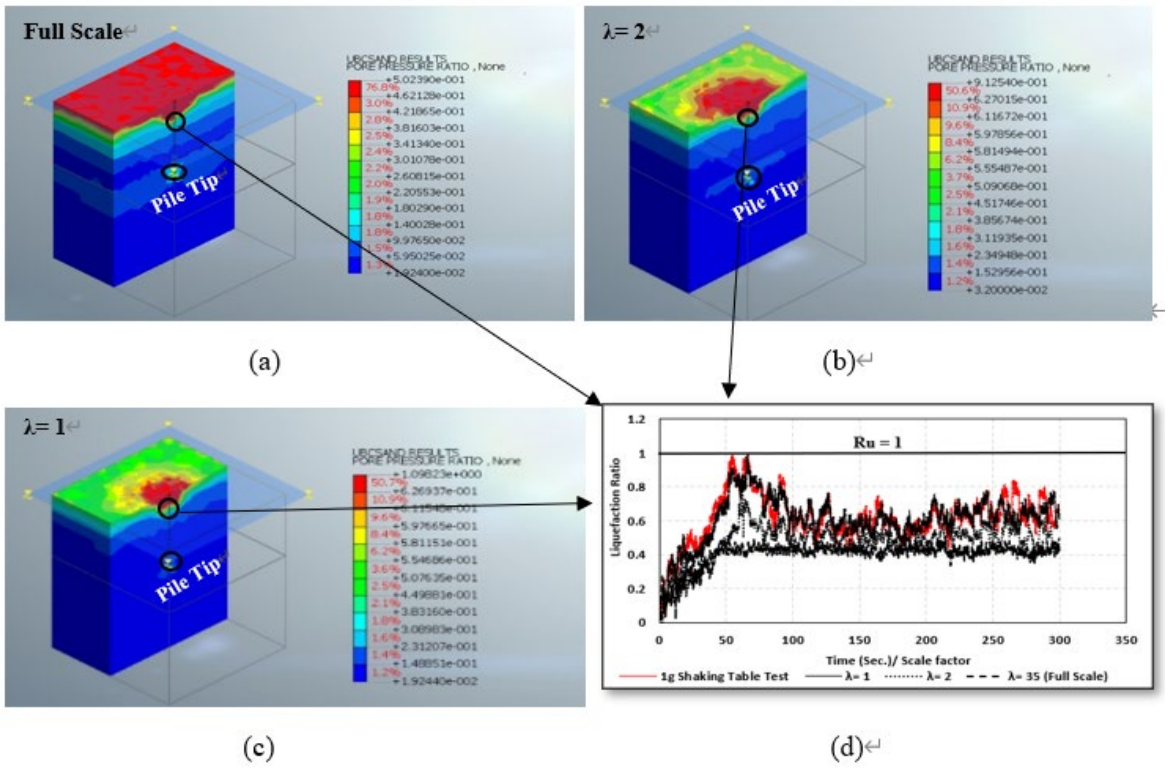

Fig. 6. Liquefaction ratio time history at a specific depth below the ground surface (at the position of maximum excess pore pressure) and under the effect of the Halabja earthquake

The time function of scales 2 and 35 was scaled down to compare the results with 1 g shaking table findings and numerical results of scale one model. According to the contour lines presented in Figs. 4, 5, and 6 of the 9 models with different acceleration histories and different scales, the liquefaction condition was developed in all models under the effect of the Kobe earthquake (very high intensity earthquake, Max. acceleration = 0.82 g) within the loose sand layer. Hence, the liquefaction ratio, Ru, was estimated by dividing the variation in pore pressure by the soil's initial vertical effective pressure. The maximum excess pore pressure reached in time between 10 and 20 seconds (Kobe earthquake), 20 and 30 seconds (Ali Algharbi earthquake), and 50 and 60 seconds (Halabja earthquake). The time for the scaling up models was multiplied by the scaling factor ($1/\lambda^{0.75}$) to compare the results with the laboratory findings of the shaking table tests. In general, pore pressure ratio decreases with increasing scaling factors, as shown in Fig. 4(a), where the excess pore pressure was significantly higher than the initial vertical effective stress at the same depth for the model of scale 1 (or 1 g shaking table findings). However, the difference between these pressures decreases with increasing scaling factor until it becomes roughly similar at λ=35. As for Ali Algharbi (Max. acceleration= 0.1 g) and Halabja (Max. acceleration = 0.102 g) earthquakes, the excess pore pressure was not enough to cause liquefaction, except in the model with λ= 1 and under the effect of Halabja earthquake. The soil model experienced liquefaction; however, the excess pore pressure was dissipated with an increasing scaling factor.

As for the soil around the pile tip, the maximum pore pressure ratio 0.27 (Kobe earthquake), 0.23 (Ali Algharbi earthquake), and 0.46 (Halabja earthquake) were captured in models with λ= 35 (full scale models) and they were not enough to develop liquefaction, as shown in Figs. 4,5, and 6. Although the liquefaction ratio showed a slight difference in the scaled models, MIDAS GTS NX effectively scaled up the shaking table tests and simulated the development of the pore pressure ratio. The minor differences may attribute to the analysis control setting, damping ratio, nonlinear soil-pile behavior, and soil multi layers interaction.

5.2 Acceleration Response and Pile Lateral Displacement

Since a crucial condition for scaling the prototype into a physical model is to achieve similar horizontal acceleration, the model behavior is governed by its gravitational mass (Hussein and El-Naggar, 2021). Thus, the gravitational mass of soil was scaled in terms of increasing soil volume by multiplying it with the scaling factor (λ^3), and the soil density was fixed to a scale factor of 1. Fig. 7 illustrated the maximum pile horizontal acceleration in dry and saturated soil layers under the effect of the three acceleration histories and the effect of the scaling model was considered as well. As for the models with scaling factors of 2 and 35, the length of the pile, which is in the z-direction, was scaled down to validate the results with the model of scale 1.

Fig. 7 shows that MIDAS GTS NX captured the acceleration trends for models under the effect of different acceleration histories and different scaling factors in saturated and dry soils. The numerical modeling shows the acceleration trends for different scaled models (under the effect of a specific acceleration history and a soil condition) are roughly similar. As for the saturated soil layers, the acceleration was decreased through the loose sand layer (from top to bottom) and then experienced little amplification through the dense sand layer. This reduction through the loose sand layer with depth may attribute to the soil softening during dynamic excitation. In the dry condition, Fig. 7 showed that the horizontal acceleration increased from the tip to the head of the pile; however, there was minor amplification in the dense sand layer (at the pile tip) under the effect of Ali Algharbi earthquake, as shown in Fig. 7(b). In general, the amplification of acceleration from bottom to top in which the peak acceleration concentrated on the pile head is in good agreement with observations of other studies (Hussein and Albusoda, 2021a; Al-Tameemi, 2018; and Chang et al., 1977). Therefore, the results of the numerical modeling in saturated and dry soil layers were acceptable.

Fig. 8 presents the lateral deformation along the pile shaft in both dry and saturated conditions under the effect of different acceleration histories and different scaling factors. For dry cases, the pile lateral displacements approach to zero (Figs. 8(a), (b), and (c)) due to soil densification which in turn restricted pile movement in terms of relative displacement (movement of a point on the pile body with respect to the lateral movement at the pile toe). However, pile lateral deformation increased significantly within the loose sand layer; particularly with higher scaled models with both soil conditions (dry and saturated). The maximum pile lateral movement was observed on the pile head due to the coupled effect of static-dynamic loading by noting the static loads (vertical and horizontal) were maintained on the pile cap as shown in Fig. 2. However, the pile experienced non-zero displacement at the toe (in the dense sand layer) when the soil condition maintained saturated and under the effects of Kobe and Ali Algharbi earthquakes, as shown in Figs. 8(d), (e).

It is important to note that the pile displacement increased nonlinearly through the loose sand layer up to the pile head in both dry and saturated conditions. The latter observation may be attributed to the soil nonuniform characteristics and the liquefied soil which moved around the pile body in saturated loose sand. Additionally, the maximum pile lateral displacement, which was noticed at the pile head, increased relatively with the scaling factors, yet by dividing these values by the scaling factor (λ), hence it was noticed that in general the lateral displacement with scales 1 and 2 is much larger than the scaled displacement of the pile in the full-scale model. Thus, the pile displacement at the head level decreased by 64.2 mm, 62.2 mm, 38.8 mm in the dry case under the effect of the Kobe earthquake for models with λ=1, 2, and 35, respectively. Table 5 presents the rest of the pile

lateral displacement results. Additionally, Fig. 9 shows that the lateral displacement of pile increased with increasing seismic intensity and this observation was noticed by Hussein and Albusoda (2021a and 2021b) when performing several 1 g shaking table tests in the laboratory to study the behavior of soil-pile interaction under the effect of Kobe, Ali Algharbi, Halabja, and El-Centro earthquakes. The lateral displacement time history (λ=1) at the pile head was validated with the 1 g shaking table test results, as presented in Fig. 9.

5.3 Pile Kinematic Response

The maximum bending moment of the scaled-up designs was lowered to the shaking table scale (λ= 1) by dividing the estimated bending moment when the scaling factor permits proper comparison with the real shaking table findings (more details are discussed by Al-Jeznawi et al., 2022b). Since MIDAS GTS NX provides the results of the bending moment divided by the unit length, and the moment definition, given as a force multiplied by length, yielded this scaling factor (i.e. $(\frac{\lambda^3}{\lambda} * \lambda)$, thus the moment scaling factor was (λ^3). Fig. 10 presents the maximum bending moment along the pile length. In general, pile experiences roughly similar trends in all models under different scales, different acceleration histories, and different soil conditions and no yielding was observed in all cases. As for the scaling effect, the scaled bending moments were slightly decreased with increasing scaling factors; i.e. the bending moment of a full scale dry model under the effect of the Kobe earthquake decreased by 17% for a model of scale 1. The rest of the results are presented in table 6.

Overall, the numerical modeling shows that the bending moment of a saturated soil condition was higher than those in a dry soil condition and the maximum bending moment reached roughly in similar positions below the ground surface. Similar observations of bending moment values were made by Hussein and El-Naggar (2021) during the investigation influence of model scale on helical pile behavior in saturated and dry soils.

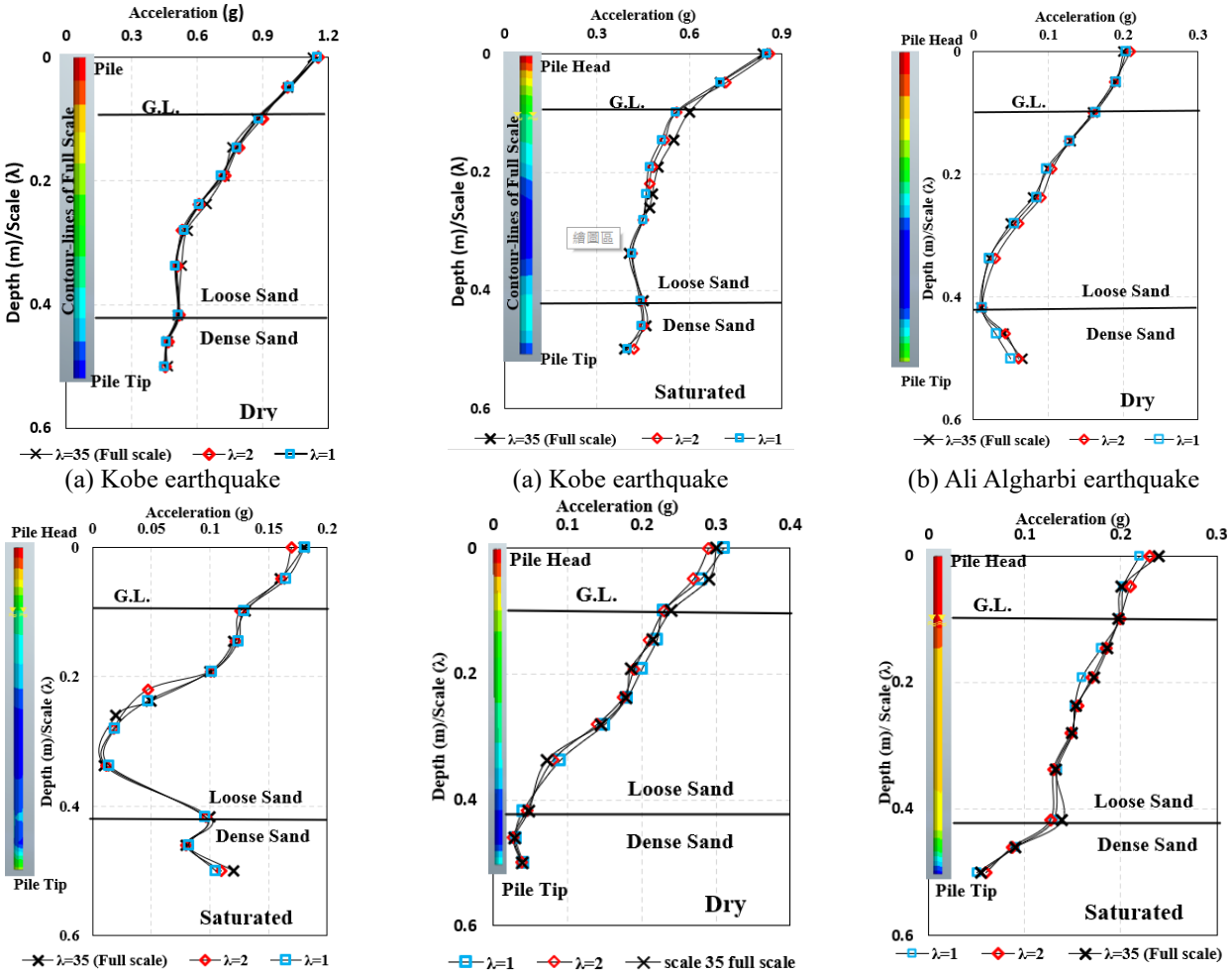

(a) Kobe earthquake (a) Kobe earthquake (b) Ali Algharbi earthquake

(b) Ali Algharbi earthquake (c) Halabja earthquake (c) Halabja earthquake

Fig. 7. Maximum pile acceleration under different acceleration histories, different scaling factors, and different soil conditions

Table 5. Summary of the maximum pile lateral deformation

Soil condition	Scale (λ)	Pile lateral displacement (mm)/ scale factor		
		Kobe Earthquake (Max. acceleration = 0.82 g)	Ali Algharbi earthquake (Max. acceleration = 0.1 g)	Halabja earthquake (Max. acceleration = 0.102 g)
Dry	1	64.2	4.1	15
	2	62.2	4	14.7
	35	38.8	2.8	9.3
Saturated	1	68.5	4.8	11
	2	67	5	10.7
	35	45.3	3.45	7.5

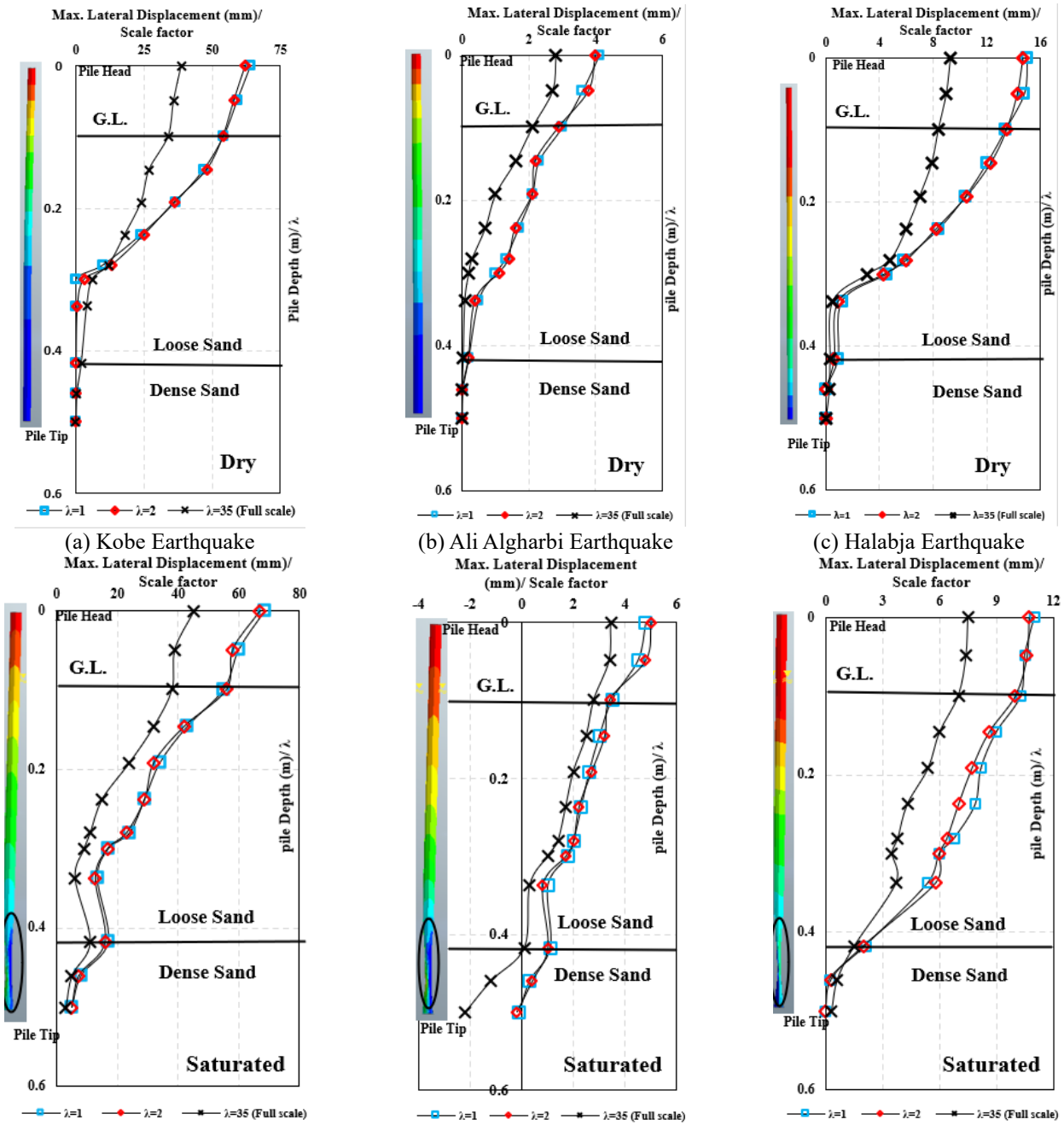

(a) Kobe Earthquake (b) Ali Algharbi Earthquake (c) Halabja Earthquake

(d) Kobe Earthquake (e) Ali Algharbi Earthquake (f) Halabja Earthquake

Fig. 8. Maximum pile lateral displacement under different acceleration histories, different scaling factors, and different soil conditions

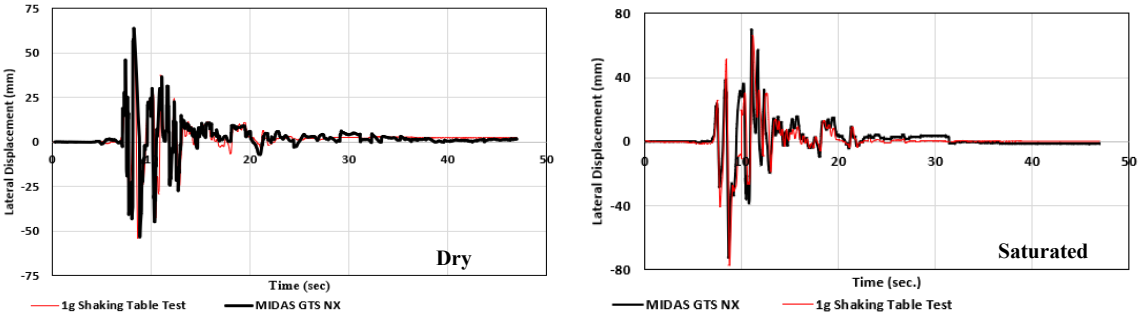

(a) Kobe earthquake

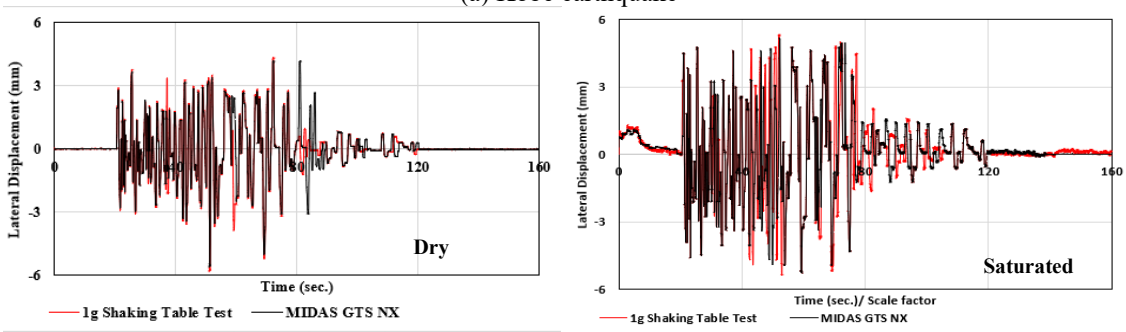

(b) Ali Algharbi earthquake

Fig. 9. Pile lateral movement time history

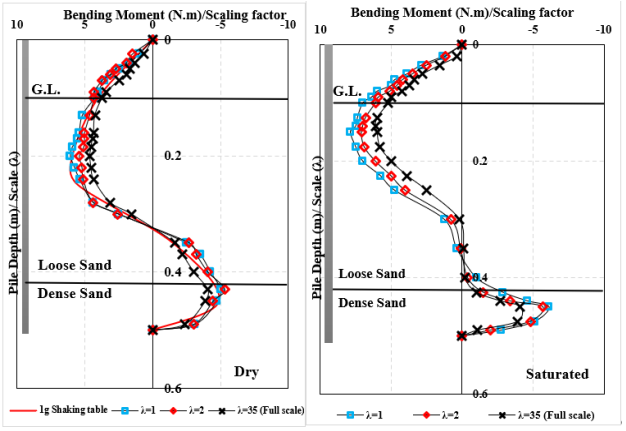

(a) Kobe earthquake

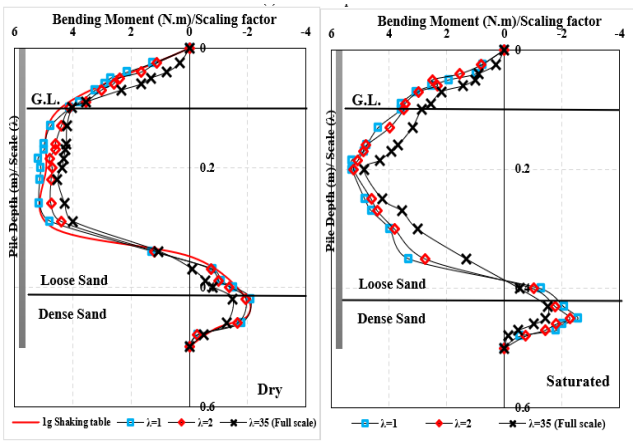

(b) Ali Algharbi earthquake

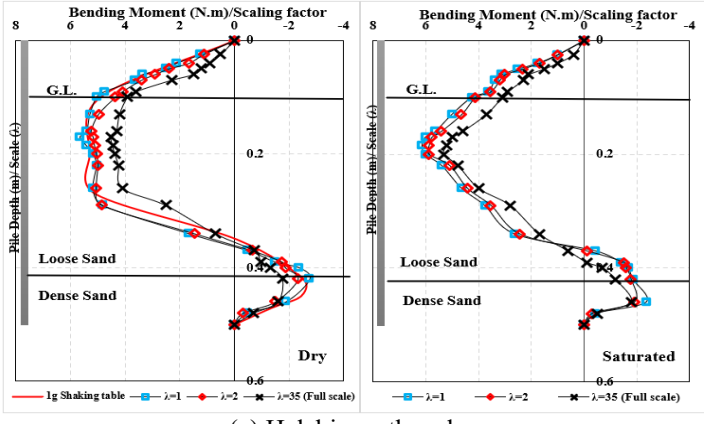

(c) Halabja earthquake

Fig. 10. The maximum bending moment along the pile length during the shaking of different acceleration histories, different scaling factors, and different soil conditions

Table 6. Summary of decreasing bending moment values with scaling up models

Soil condition	Scale (λ)	Percentage of decreasing the scaled bending moment		
		Kobe Earthquake (Max. acceleration = 0.82 g)	Ali Algharbi earthquake (Max. acceleration = 0.1 g)	Halabja earthquake (Max. acceleration = 0.102 g)
Dry	2	10	7	8.5
	35	23	14	19
Saturated	2	6.5	0.9	1.5
	35	18.6	9	14.7

5.4 Pile Axial Response

Significant settlements have been linked to many infrastructure and building disasters during earthquakes (Tokimatsu and Asaka, 1995). Piles set in saturated sand layers may display unique techniques based on the excess pore pressure generated within the loose sand, as such effective vertical stress and, as a result, the soil shear stiffness diminishes. Furthermore, the friction resistance of the end bearing and pile body will be impacted in distinct ways. When the excess pore pressure in the bearing stratum rises, the pile may settle significantly, causing higher end bearing capacity to be mobilized shaft friction, on the other hand, decreases with excess pore pressure formation and may even disappear when liquefaction develops. Dry-site piles, however, have a different damage pattern. The pile may be subjected to severe tension and compression phases, and its settlement may occur during periods of strong acceleration. Nevertheless, pile settlement is lower than in saturated areas, and bearing capacity collapse is unlikely since soil properties may increase as a result of compaction. The influence of model scale in the shaking table on closed ended pipe pile settlement, frictional resistance, and shear stress-strain relationship for both saturated and dry models are discussed below.

Fig. 11 shows the time history of the pile vertical movement in both moist and dry models. Unrelatedly to the model scale and acceleration histories, the saturated models had significantly higher settlements than the dry models. Furthermore, the settlement outcomes were standardized to the scaling factor (λ) so that the multiple scaled models could be compared simply. Through both saturated and dry investigations, the pipe pile settlement expanded as the model scale increased; yet, the scaled settlement dropped with full scale models. Additionally, the pile settlement decreased with decreasing seismic intensity; i.e. the maximum scaled settlement dropped to 3.8, 0.31, and 4.1 in dry models, and 12.2, 0.35, and 6 in the saturated models for Kobe (0.82 g), Ali Algharbi (0.1 g), and Halabja (0.102 g) earthquakes, respectively. Meanwhile, the pile settlement trends were roughly similar for different scales under the effect of a particular acceleration history and a soil condition, and the settlement time was scaled by a factor of ($\lambda^{0.75}$), in accordance with the specified time scale factor (Wood, 2004).

The frictional resistance along the pile length was determined by the tangential stresses of the interface elements along the pile body. Hussein and El-Naggar (2021) investigated the frictional resistance along with the helix piles by integrating their shear stresses. It is worth noting that in general the frictional resistance become higher in a dense sand than in a loose sand layer regardless of the effect of scaling, acceleration history, and soil condition as shown in Fig. 12. The latter may be attributed to the high excess pore pressure ratio at shallow depth and the shorter length of the shear zone in the loose sand layer.

The findings demonstrate that the frictional resistance followed the same pattern regardless of the effect of scaling. At early stages, these values increased with increasing seismic intensity; i.e., Fig. 12(a) shows that the pile frictional resistance at early stages under the effect of the Kobe earthquake (0.82 g) was roughly 65 kPa and 66 kPa and they become 48 kPa and 28 kPa under the effect of Ali Algharbi earthquake (0.1 g) for dry and saturated soils, respectively. Overall, the frictional resistance values were increased by increasing the model scale; i.e., frictional resistance under the effect of the Kobe earthquake in dry soil increased from 65 kPa and 120 kPa to 2261 kPa as in the scale 1, 2, and 35 respectively. Hussein and Albusoda (2021) noticed that the soil particles lose their shear strength and roughly act as a slurry during dynamic excitation. In addition, in models of full scale (λ=35), it is worth noting that the frictional resistance values were significantly decreased at the final stage; i.e., it decreased from 2241 kPa to -3.8 kPa under Kobe earthquake in a saturated soil sample. Table 7 presents a summary of the frictional resistance at the early and final stages in the ground surface level. Table 8 presents a summary of the frictional resistance at the early and final stages at the pile tip. From tables 7 and 8, it could be noticed that the pile frictional resistance in the dry soils is much higher than those in the saturated cases, which may attribute to the effect of the development of the excess pore pressure in saturated soils. Additionally, the maximum frictional resistances were observed at the pile tip which may attribute to the pile settlement during seismic excitation which in turn mobilize the end bearing capacity.

Thus, because of the kinematic soil-pile interaction, the nonlinear soil reaction, and opposing kinematic and inertial factors, scaling the pile axial seismic performances is complicated. Fig. 13 shows the shear stress- shear strain relationship and the maximum and minimum cycles to a soil element adjacent to the pile body at depth of 3.5 m in the full-scale model. For dry conditions, the results were in a good agreement with the previous studies performed by Susumu Iai (1989) and Thilakasirim (2010).

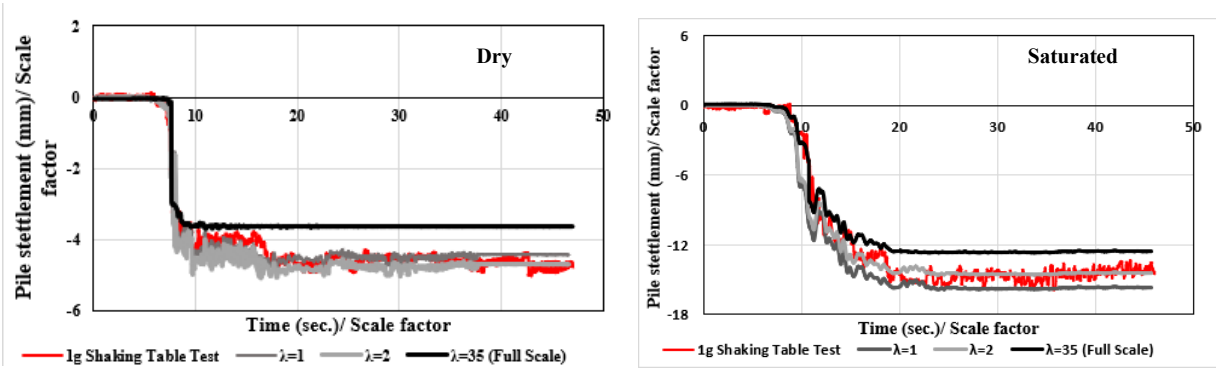

(a) Kobe earthquake

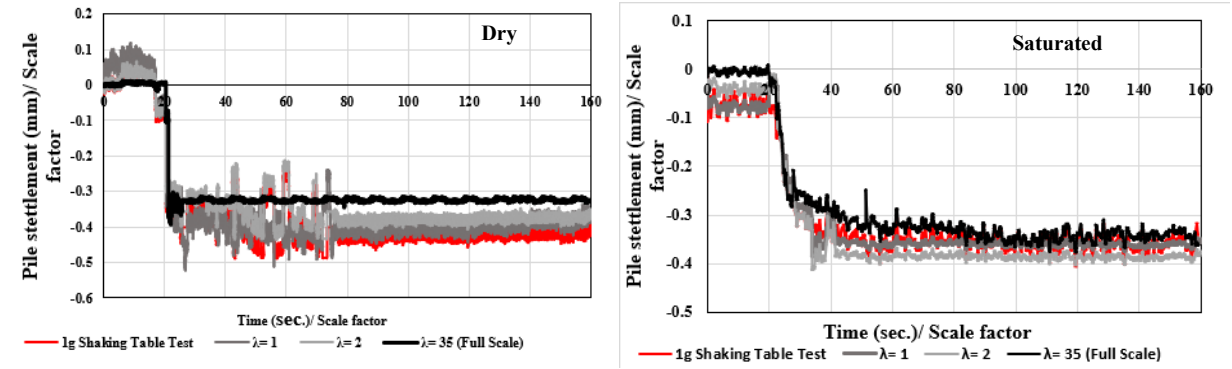

(b) Ali Algharbi earthquake

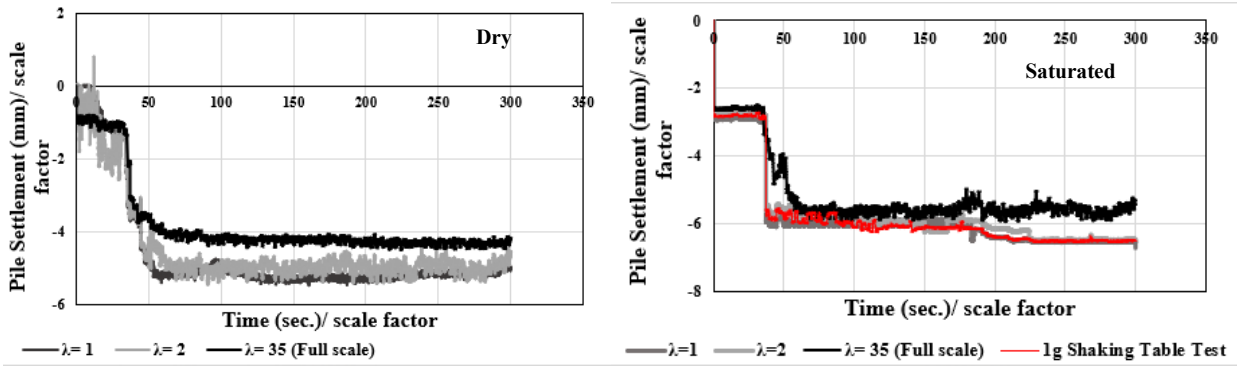

(c) Halabja earthquake

Fig. 11. The maximum pile settlement during the shaking of different acceleration histories, different scaling factors, and different soil conditions

Table 7. Summary of frictional resistance at the early and final stages during dynamic excitation at the soil level.

Frictional Resistance kPa @ Early Stages on the Ground Surface Level						
	Kobe		Ali Algharbi		Halabja	
Model Scale	Dry	Saturated	Dry	Saturated	Dry	Saturated
1	65	65.8	26.1	28.4	28.6	29.3
2	120	128	48	55.3	56.3	57.4
35 (Full Scale)	2261	2241	906	993	983	1063
Frictional Resistance kPa @ Final Stage on the Ground Surface Level						
	Kobe		Ali Algharbi		Halabja	
Model Scale	Dry	Saturated	Dry	Saturated	Dry	Saturated
1	-65.1	-0.1	-29.2	-17.6	-37.5	-30.8
2	-121	-0.11	-54.7	-34.5	-70.9	-30.8
35 (Full Scale)	-1411	-3.8	-550	-304	-510	-452.6

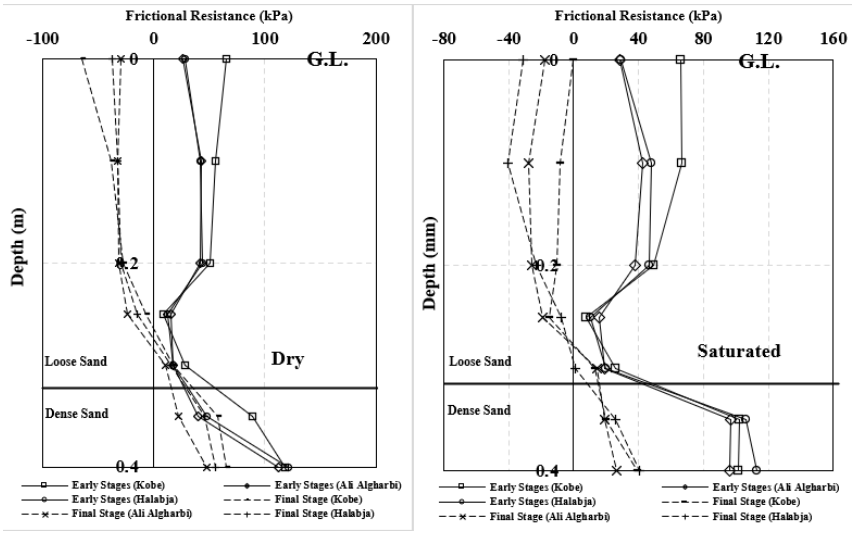

(a) Scale 1

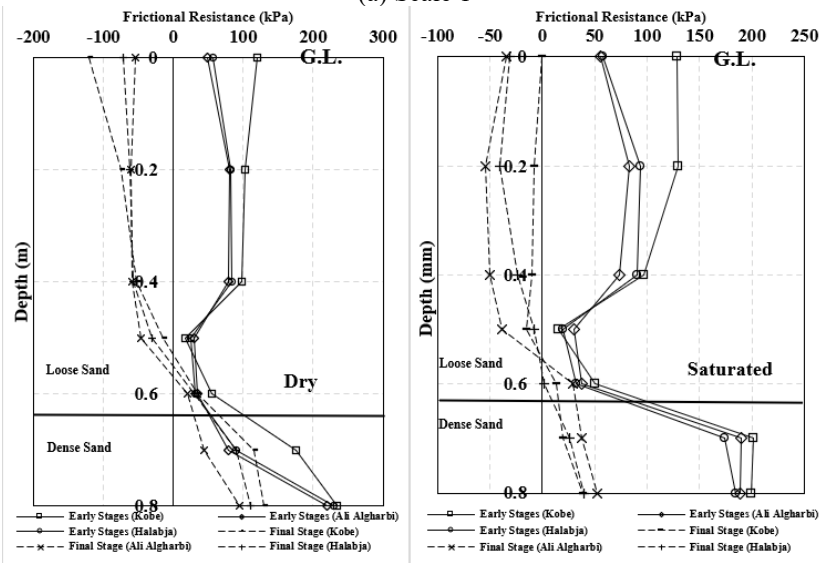

(b) Scale 2

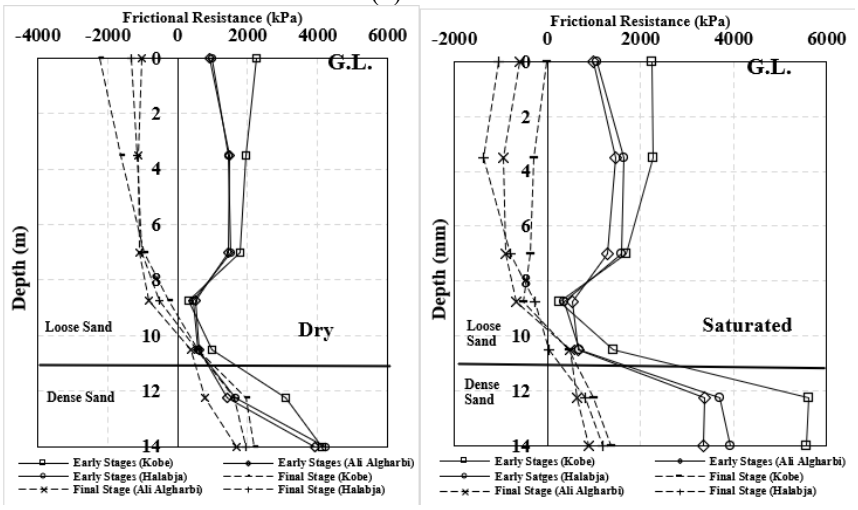

(c) Scale 35 (Full scale)

Fig. 12. Frictional resistance along the pile length during the shaking of different acceleration histories, different scaling factors, and different soil conditions.

Table 8. Summary of frictional resistance at the early and final stages during dynamic excitation at the pile tip.

Frictional Resistance kPa @ Early Stages near the pile tip						
	Kobe		Ali Algharbi		Halabja	
Model Scale	Dry	Saturated	Dry	Saturated	Dry	Saturated
1	118	101	112	96	120	112
2	234	199	219	189	229	184
35 (Full Scale)	4124	5565	3908	3363	4218	3931
Frictional Resistance kPa @ Final Stage near the pile tip						
	Kobe		Ali Algharbi		Halabja	
Model Scale	Dry	Saturated	Dry	Saturated	Dry	Saturated
1	65	38.9	48	26	56	40
2	130	38.92	94	52	110	39.7
35 (Full Scale)	2190	1357	1672	890	1956	1202

As for the saturated sand soils, the liquefaction model (UBCSAND) intends to replicate the main features during seismic excitation (Chou et al., 2021) which is in turn, called the 'Banana loop' during such shear stress reversal (from positive values to negative and vice versa). Consequently, the results show that the stresses in dry cases are much higher than those in the saturated ones.

As a summary, the results showed that the scaled-up models had the same lateral and vertical response as the original 1 g shaking table models. Nevertheless, there were some indications of dissimilarity in the scaled modeling techniques, that could make extrapolating shaking table observations to the full scale difficult. Statistical analysis was used to analyze the variation of the obtained results using various acceleration histories, model scales, and soil conditions. As shown in Fig. 14, the maximum lateral movements along with the pile depth, maximum pile settlement, and maximum frictional resistance at the ground surface were normalized to those in the model scale 1:1 ratio. This normalization helps to describe the variation in findings according to the model scale and gives a good insight into extrapolating shaking table laboratory results to numerical full-scale model.

The normalized maximum lateral pile displacement (at the pile head) is presented in Fig. 14(a). In saturated cases, the pile displacements are higher than in dry conditions. In general, the pile lateral settlement was less than the soil deformation in a saturated model which may be due to the rearrangement of the soil particles during vibration around the pile body during the development of the excess pore pressure ratio. In comparison to the dry model, the displacement values in the saturated models were closely related to the geometric scale factor (λ). This would be illustrated by Iai (1989) and wood (2004) scaling laws, which states that the displacement scale factor is determined by the strain and length factors (i.e., $\lambda\lambda_\epsilon$). Since, the liquefiable model has a higher strain level than the dry one, which could show the disparity between the dry and saturated models. Hence, as the soil liquefies, the pile behavior is governed by the well-controlled pile flexural rigidity. The pile performance in the dry model, however, is influenced by the pile and soil parameters, including the kinematic coupling of the pile-soil combination. During shaking, these various components may have conflicting actions.

As for the vertical response of the pile, Fig. 14(b) and (c) show the vertical displacement factor and frictional resistance factor that both influence the axial response of the pile. The normalized pile settlement factor (Fig. 14(b)) illustrated that the pile settlement factor increases with scaling up model (λ); and the frictional resistance stresses at the pile body and the pile tip (Fig. 14(c)) demonstrated that the pile frictional resistance in the saturated models is diminished with seismic excitation. It is worth mentioning that, the pile frictional resistance has generally similar trend in both saturated and dry models.

6. CONCLUSION

This study implemented 3D finite element models to study the soil-pile interaction attitude under the effect of coupled static-dynamic loading and validated the main results with 1 g shaking table tests (done by Hussein and Albusoda, 2021a, and 2021b). An Aluminum pile with dry and saturated sand soil (Karbala'a sand) has been used in the laboratory and the software input parameters were calibrated according to the modified Mohr-Coulomb model (for dry soil model) and modified UBCSAND model (for saturated soil model). Furthermore, free field elements were created around the model sides (in the direction of applied ground motion) and elastic boundary conditions were used at the bottom of the model in order to reduce the wave reflection to the lateral response and the interference of the model based on the vertical response. Thus, three different acceleration histories (Kobe, Ali Algharbi, and Halabja) and three different scales (1, 2, 35 "full scale") were used in this study, and the time of ground shaking was scaled up based on Wood (2004). The verified finite element models were employed to inclusively discuss the effect of acceleration histories, scaling, and soil conditions on the soil-closed-ended pipe pile lateral and vertical performance.

In both the saturated and dry experiments, horizontal pile acceleration developed identically in the scaled models, and the findings of scaled-up models showed the same patterns

in the vertical and lateral responses. Regardless of the effect of the model scale, acceleration history, and soil condition, horizontal ground acceleration was increased from bottom to top of the pile during shaking until it reaches the maximum value at the pile cap. The liquefaction ratio was increased by increasing the seismic intensity, the maximum liquefaction ratio was observed with the model of scale 1:1 ratio under the effect of Kobe earthquake (0.82 g). Yet with the full-scale model, the liquefaction ratio decreased significantly; i.e., it was decreased from 1.64% (λ=1) to 1.04% (λ=35) in the same mentioned model. In general, the pile lateral deformation was less than the soil lateral deformation and pile deformation factor was higher in saturated models than the dry models. The pile experienced a significant deformation in the saturated dense sand layer due to the all-around soil compression pressures during shaking, this was observed in the full-scale model as shown in Fig. 8(d), (e), and (f). Shear stress reversal "Banana loop" was captured by both the modified Mohr-Coulomb model and the modified UBCSAND model for an element slightly below the ground surface (at maximum liquefaction development). The development of stresses in dry cases is in general higher than those in saturated models.

Regardless of the model size, acceleration history, and soil condition; the position of the maximum bending moment of the pipe pile was roughly identical when compared with the 1 g shaking table tests and the scale 1 model. Regardless of the acceleration history, the saturated models had a larger vertical deformation factor than the dry models. In general, the frictional resistance at the pile tip was slightly higher than the frictional resistance around the pile body, and the frictional resistance factor on the ground surface of dry models was slightly higher than those of saturated models.

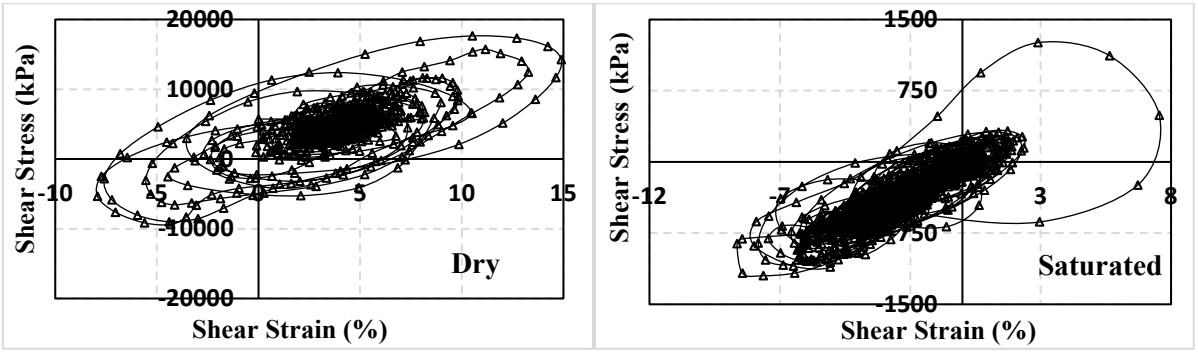

(a) Kobe earthquake

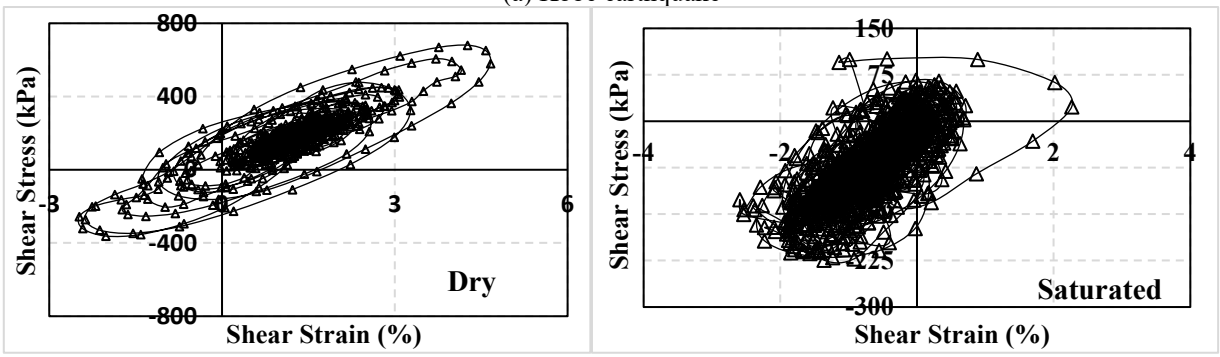

(b) Ali Algharbi earthquake

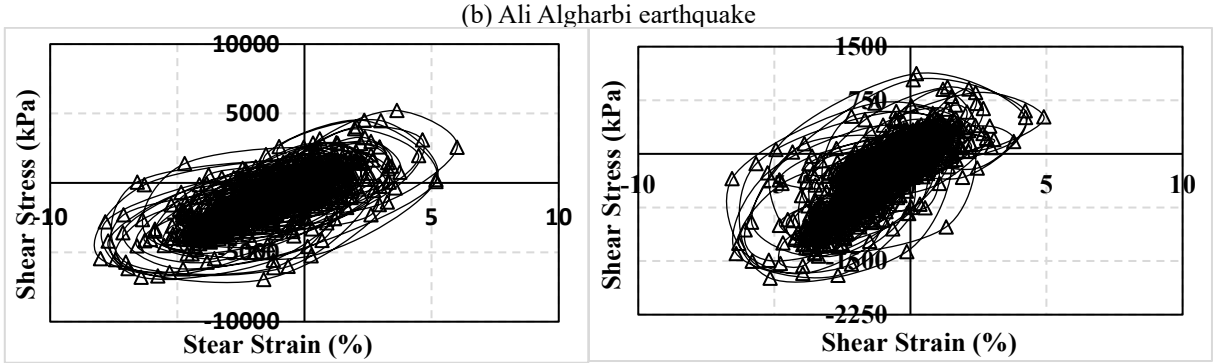

(c) Halabja earthquake

Fig. 13. An undrained cyclic loading response of sand soil under a coupled of static loads (vertical and lateral) and dynamic excitation

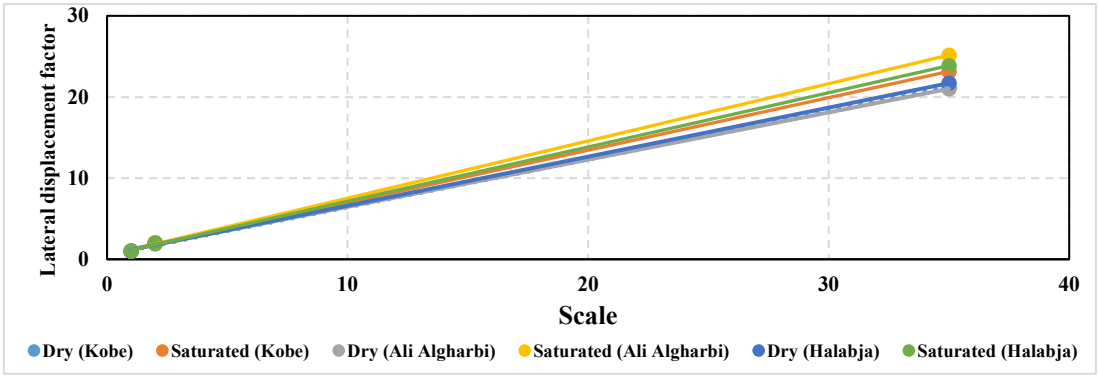

(a)

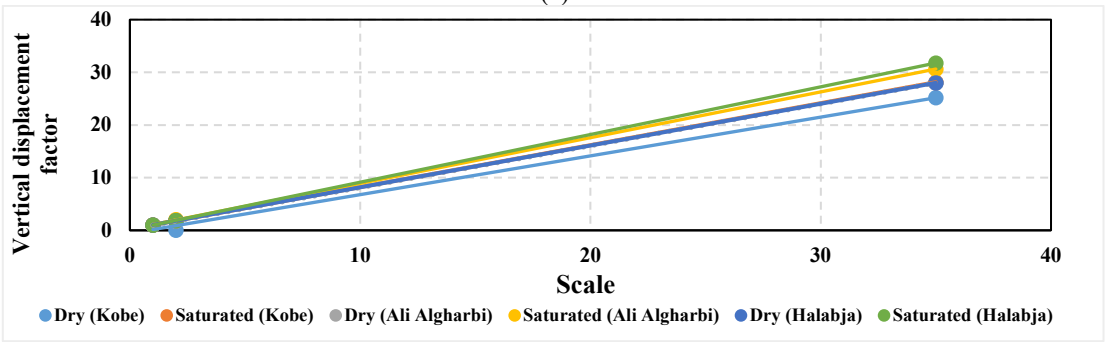

(b)

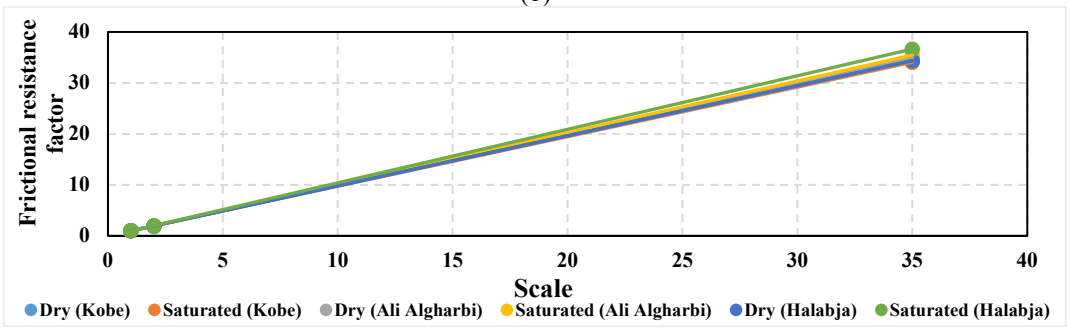

(c)

Fig. 14. Results of normalization analysis: (a) pile lateral displacement; (b) pile vertical movement; and (c) frictional resistance stresses

REFERENCES

Al- Tameemi, S., 2018. Experimental and numerical study on the effect of liquefaction potential of piles in sandy layers of soil under earthquake loading. Ph.D Thesis, Civil Engineering Department, University of Al-Nahrain.

Al-Ghanim, A., 2019. Behavior of geogrid-pile foundation system in loose sandy soils under Halabjah earthquake. International Journal of Geomate, 17, 267–276.

Al-Ghanim, A., Shafiqu, Q.S.M., Ibraheem, A.T. 2019. Finite element analysis of the geogrid pile foundation system under earthquake loading. Al-Nahrain Journal for Engineering Sciences NJES 22, 202–207.

Al-Jeznawi, D., Jais, I.B., Albusoda, B.S. 2022a. The slenderness ratio effect on the response of closed-end pipe piles in liquefied and non-liquefied soil layers under coupled static-seismic loading. Journal of the Mechanical Behaviors and Materials, Accepted.

Al-Jeznawi, D., Jais, I.B., Albusoda, B.S. 2022b. A soil-pile response under coupled static dynamic loadings in terms of kinematic interaction. Journal of the Civil and Environmental Engineering, Accepted.

Al-Salakh, A.M., Albusoda, B.S. 2020. Experimental and theoretical determination of settlement of shallow footing on liquefiable soil. Journal of Engineering 26.

ASTM (D 1586-99): Standard test method for penetration test and split-barrel sampling on soils (D 1586-99), Annual Book of ASTM Standards, 04.08, American Society of Testing and Material, Philadelphia.

Almashhadany, O.Y., Albusoda, B.S. 2014. Effect of allowable vertical load and length/ diameter ratio (l/d) on behavior of pile group subjected to torsion. Journal of Engineering, 20.

Chang, C.A., Lin, H.D., Lo, C.C. 1977. Tests of pattern change for automated detection of printing faults using computer vision systems. International Journal of Industrial Engineering, 4, 5–13.

Chou, J.C., Yang, H.T., Lin, D.G., 2021. Calibration of finn model and ubcsand model for simplified liquefaction analysis procedures. Appl. Sci. 11, 528. doi.org/10.3390 /app11115283.

Dong, J., Chen, F., Zhou, M., Zhou, X., 2018. Numerical analysis of the boundary effect in model tests for single pile under lateral load. Bull Eng Geol Environ;1057, 1068–77.

Ebeido, A., Elgamal, A., Tokimatsu, K., Abe, A., 2019. Pile and pile-group response to liquefaction induced lateral spreading in four large-scale shake-table experiments. Journal of Geotechnical and Geoenvironmental Engineering: 4019080–145.

Hussein, A.H., El Naggar, M.H., 2021. Effect of model scale on helical piles response established from shake table tests. Soil Dynamic and Earthquake Engineering, 152, 107013.

Hussein, R., Albusoda, B., 2021a. Experimental and numerical analysis of laterally loaded pile subjected to earthquake loading. In Modern Applications of Geotechnical Engineering and Construction, 291–303. Springer, Singapore.

Hussein, R., Albusoda, B., 2021b. Experimental modelling of single pile under combined effect of axially and laterally loadings in liquefiable soil. Geotechnical and Geological Engineering. Accepted.

Iai, S., 1989. Similitude for shaking table tests on soil-structure-fluid model in 1 g gravitational field. Soils Foundation. 105–118–29.

Michael, H., Beaty and Peter, M., Byrne, 2011. Documentation report: ubcsand constitutive model on itasca udm web site.

Oh-oka, H., Iiba, Abe, A., Tokimatsu, K., 1996. Investigation of earthquake-induced damage to pile foundation using televiewer observation and integrity sonic tests. (In Japanese) Tsuchi-tokiso, 44, 3, The Japanese Geotech. Soc.

Robinsky, E., Morrison, C., 1964. Sand displacement and compaction around model friction piles. Canadian Geotech J. 81. 93–1.

Takashi, T., Gazatas, G., 1996. Pile foundations subjected to large ground deformations: lessons from Kobe and research needs. 11th World Conference on Earthquake Engineering, Elsevier Science Ltd.

Thilakasirim, H.S., 2010. Kinematic and inertial effects of earthquakes on rock socketed single piles in a two-layered medium. Journal of the Institution of Engineers, Sri Lanka, 43, 3.

Tokimatsu, K., Asaka, Y., 1995. Effects of liquefaction-induced ground displacements on pile performance in the Hyogoken-Nambu earthquake. Soils Foundation;163. 177–38.

Tokimatsu, K., Suzuki, H., Sato, M., 2004. Effects of inertial and kinematic forces on pile stresses in large shaking table tests. Proc., Proc., 13th World Conf. on Earthquake Engineering, Vancouver.

Wood, D.M., 2004. Geotechnical modelling, CRC press.

Yasuda, S., Ishihara, K., Morimoto, I., Orense, R., Ikeda, M., Tamura, S., 2000. Large-scale shaking table tests on pile foundations in liquefied ground. Proc., 12th World Conf. on Earthquake Engineering, Citeseer. 1474.